

***JHK'* Imaging Photometry of Seyfert 1 AGNs and Quasars II:
Observation of Long-Term Variability**

Keigo Enya¹, Yuzuru Yoshii^{1,4}, Yukiyasu Kobayashi², Takeo Minezaki¹, Masahiro
Suganuma³, Hiroyuki Tomita³ and Bruce A. Peterson⁵

¹ Institute of Astronomy, School of Science, University of Tokyo, Osawa 2-21-1, Mitaka,
Tokyo 181-8588, Japan

² National Astronomical Observatory, Osawa 2-21-1, Mitaka, Tokyo 181-8588, Japan

³ Department of Astronomy, University of Tokyo, Hongo 7-3-1, Bunkyo-ku, Tokyo
113-0033, Japan

⁴ Research Center for the Early Universe (RESCEU), School of Science, University of
Tokyo, Hongo 7-3-1, Bunkyo-ku, Tokyo 113-0033, Japan

⁵ Research School of Astronomy and Astrophysics, The Australian National University,
Weston Creek, ACT 2611, Australia

Received _____; accepted _____

ABSTRACT

Observations of 226 AGNs in the near-infrared J , H , and K' bands are presented along with the analysis of the observations for variability. Our sample consists mainly of Seyfert 1 AGNs and QSOs. About a quarter of the objects in each category are radio loud. The AGNs in the entire sample have the redshifts spanning the range from $z = 0$ to 1, and the absolute magnitudes from $M_B = -29$ to -18 . All the objects were observed twice and their variability was measured by differential photometry.

A reduction method of differential photometry, optimized to the analysis of extended images, has been developed. The systematic error in variability arising from AGNs of highly extended images is estimated to be less than 0.01 mag in each of the J , H , and K' bands. The systematic error arising from the flat fielding is negligible for most AGNs, although it is more than 0.1 mag for some particular cases. The overall average flat fielding error is 0.03 mag for the image pairs. We find that these systematic errors are superseded by statistical errors, and the overall average total systematic and statistical errors amounts to 0.05 mag in the measured variability in each band.

We find that 58% of all the AGNs in the entire sample show variability of more than 2σ , and 44% of more than 3σ . This result holds independent of the J , H , and K' bands. The detection rate of variability is higher for a subsample of higher photometric accuracy, and there appears no limit to this tendency. In particular, when we consider a subsample with small photometric errors of $\sigma < 0.03$ mag, the rate of 2σ detection is 80%, and 64% for 3σ detection. This suggests that most AGNs are variable in the near-infrared.

Subject headings: galaxies: active—quasars: general—galaxies: photometry

1. Introduction

Active Galactic Nuclei (AGNs) emit enormous amount of energy from their central, compact region. However, it is impossible to resolve this compact region with current instruments when the AGNs are at cosmological distances. Observation of variability for such distant objects is a useful method for investigating the emitting mechanism as well as the internal structure of the compact region. Therefore, a first pathway to progress is to detect their variability in various passbands and to study the detected variability in detail. In this regard, it is essential to measure not only the magnitude of variability but also its error as accurately as possible.

Recent monitoring observation of AGNs by differential photometry with CCDs detected variability in almost all of the AGNs observed in the optical bands (Borgeest & Schramm 1994, Netzer et al. 1996, Giveon et al. 1999). Determination of near-infrared (NIR) variability in AGNs, for which optical variability has already been detected, leads to a better understanding of their emission mechanisms. In the dust reverberation model, the structure of the dust torus can be investigated from the time delay of the NIR variability, which lags behind the UV/optical variability (Cravel, Wamsteker & Glass 1989, Barvanis 1992).

Neugebauer et al. (1989) monitored 108 optically selected quasars in the J , H , K , L and $10\mu\text{m}$ bands, and discussed the probability of each AGN having varied. However, the number of AGNs with NIR variability measurements of comparable accuracy to the optical study, is still too small to derive general properties of variability. Therefore, it is of prime importance at this stage to obtain more data of high accuracy on NIR variability.

Here, in this paper, we present the new JHK' variability data for 226 AGNs. To date, this is the largest sample systematically observed in the NIR. Each AGN was observed twice. Efficient and highly accurate detection of variability was achieved using differential

photometry. The method of error estimation and the generality of the phenomenon of variability are discussed in this paper. Various relations among detected variability, absolute B -magnitude and AGN redshift will be discussed in Paper III.

We have been conducting a project called MAGNUM which is an acronym for Multicolor Active Galactic Nuclei Monitoring (Kobayashi et al. 1998a, 1998b). The MAGNUM Project aims to determine the distances to many AGNs from measurements of the time delay between NIR and UV/optical variabilities. This paper is therefore a preliminary target selection of AGNs with sizable variability, which will be monitored by the MAGNUM Project.

2. Observations

The data analyzed in this paper was obtained using the image reduction processes described in §2 of Paper I. We selected 226 AGNs from the catalogs of Quasars and Active Galactic Nuclei (Veron-Cetty and Veron 1993, 1996, 1998), which will also be used as target AGNs for the MAGNUM Project. Their right ascensions and declinations are shown in Fig.1 of Paper I, and their redshifts and absolute B -magnitudes in Fig.2 of Paper I.

All observations were performed with the NIR camera PICNIC (Kobayashi et al.1994) mounted on the 1.3m infrared telescope at the Institute of Space and Astronomical Science (ISAS), Japan. AGNs were imaged by stepping the telescope in a raster pattern. Two standard stars at different altitudes were observed three times each night in the J , H and K' bands. In usual cases, images were reduced automatically by the software PICRED developed for the PICNIC camera and optimized for the reduction of AGN and QSO images.

3. Analysis

3.1. Differential photometry for detecting the variability of AGNs

3.1.1. The problems of standard star-based photometry

Each of AGNs was observed on two different nights with photometric standards. However, some problems arise when one wishes to regard the difference between two measured magnitudes as variability.

One of the problems arises from different the PSFs for AGNs and the photometric standards which occur due to variation of seeing and/or telescope tracking. Adopting a larger aperture alleviates this problem, but at the same time it decreases the S/N ratio of an object image. The S/N ratio increases by increasing the integration time, but longer integration time obviously decreases the number of observable objects per night.

Another problem arises from the different atmospheric transmissivities at the different times when the AGNs and the photometric standards were observed. Frequent observation of photometric standards alleviates this problem, but at the same time it decreases the observational efficiency. The atmospheric transmissivity as well as the seeing conditions could vary significantly, especially when a cloud comes into the line of sight. Great care was taken to avoid such intervening clouds during the observations, but some very thin clouds were identified only after daybreak. The data taken on such nights and those on non-photometric nights were excluded from the analysis, which also leads to a loss of observational efficiency.

The above problems stem from magnitudes of images taken on different nights, along different lines of sight, and under different instrumental conditions such as the tracking of the telescope. Unless these problems are avoided, the standards-based photometry is not an

accurate method for detecting the variability of AGNs.

3.1.2. The superiority of differential photometry for variability detection

In principle, the above problems from variations of PSF and transmissivity are minimized by differential photometry. Therefore, we adopted a method of differential photometry in order to detect the variability of AGNs with high accuracy and reliability. In the ideal case such that target AGNs and nearby reference objects are point sources and no errors exist in flat fielding, we describe the scheme of differential photometry which is used to detect the variability of AGNs.

We measure instrumental aperture magnitudes of both AGNs and reference objects on two different nights. We regard their magnitude difference as reflecting real difference of their fluxes, because the systematic errors from variations of seeing and telescope tracking are cancelled out under the assumptions that the PSFs in each field are the same within the required accuracy and that variation of atmospheric transmissivity equally affects all objects in each field. We therefore regard the change of measured magnitudes from different nights for each AGN as its variability. Cancellation of systematic errors in the case of differential photometry justifies our use of a smaller aperture, which results in smaller statistical errors as well. It is worth mentioning that a high observational efficiency is maintained by differential photometry, because the data taken through thin clouds can also be used.

There remain some systematic errors that are not suppressed even by differential photometry. Imperfect of flat fielding gives rise to errors in the magnitude difference between an AGN and its nearby reference objects. Variation in the PSF is not completely canceled if intrinsic brightness profiles are not the same. Furthermore, the possible variability of the

reference objects, of course, is another source of error in determination of the variability of the AGN.

However, as describe below, all these errors were not fatal in our analysis, where the images of AGNs are not very extended and most reference objects consist of stars.

3.1.3. The use of DSS images as positional reference

Identification of AGNs and reference objects observed on two different nights is an important step in differential photometry. We used images from a digitized Palomer chart, or equivalently, the Digitized Sky Survey (DSS), as positional references. The identification of each object on three frames, such as a DSS frame and two NIR frames taken on different nights, is more reliable than only on two NIR frames.

The DSS images of all AGNs observed in this paper were obtained with a batch script from a database at the Data Analysis Center of the National Astronomical Observatory, Japan (NAOJ); DDS2 images are of better resolution compared to those of DSS1. We use as many DSS2 images as possible, while not excluding the use of DSS1 images for the purpose of completeness. The size of the extracted DSS images was 12×12 arcmin². That size is larger than the mosaiced NIR images we obtained.

Objects in the DSS images were automatically detected by the IRAF `cl` script which consists of the DAO find task and a perl script. After some trial-and-error tuning of the detection parameters, we found that objects are distinguished from noise more easily in the DSS images than in our NIR images.

Associating each target AGN with a DSS image was done manually. The target was mostly located at the center, with some exceptions where it was a little away from the center owing to positional errors. The finding charts were prepared based on the information in

the VV catalog. For efficient association, the `cl` script was prepared and used in such a way that the nearest object from mouse-clicked point was searched. The found object was, if close enough, regarded as the target AGN, otherwise an error message of ‘not found’ was given. The result of detection/non-detection of AGNs and nearby reference objects were written in a text file within other additional information.

3.1.4. The detection of objects in NIR images

Objects in the NIR images were automatically detected using the `cl` script similarly to the case for the DSS images. Luminosity of our AGNs is distributed over a wide range, so that a large number of noise images were detected when the threshold was set low enough to detect faint AGNs. In such a case, many false detections emerge near the faint end of the detected object distribution. An appropriate level of faint object detections was estimated and the faint object distribution was automatically smoothed with the IRAF task for image replacement. By this operation, false detections were greatly decreased, though not completely excluded.

Together with nearby reference objects, most AGNs were detected in the automatic detection scheme, while some of faint AGNs required manual trial-and-error tuning of the detection parameters. However, invisible AGNs, or very faint AGNs that were not detected by any manual method were regarded as non-detections.

The most central object was not always the target AGN in the NIR images, partly because the tuning of the telescope pointing was not done for some time. Furthermore, since the fourth quadrant of the detector was out of order in the second of the two observation periods, an off-center region of the detector was used to detect the AGNs in the second periods. Therefore it was necessary to identify and mark the target AGNs manually using

the finding charts.

3.1.5. The identification of reference objects

It was necessary to identify reference objects automatically, because their number exceeds that of AGNs by about an order of magnitude and is beyond ability of manual operation. The DSS and NIR images were listed downwards from the top, and arranged according to their coordinates from north to south. The coordinates of detected objects or AGNs in such images were then transformed to the new coordinates in units of arcsec, placing each AGN at the origin. Identification between the DSS and infrared images was performed by a usual least-squares fitting with two free parameters of rotation and expansion of the images. At the first step of the fitting, reference objects in the NIR images and those in the DSS images, if within a separation of 10 arcsec, were regarded as the same objects.

The fitting was iterated with a smaller aperture using new starting parameters which were obtained as the result of the last iteration. The lower limit for decreasing the aperture was set to be 2 arcsec, which is comparable to a typical FWHM for a point source in the NIR images. The final value of rotation parameter was less than a few degrees, and that of the expansion factor was about 1 ± 0.05 for most cases. The automatic fitting was almost always successful, and the script produced from the last iteration was useful. For some cases where only very faint objects were detected in the images, the iteration did not show a tendency of convergence, so that manual operation was needed to tune the parameters. However, if even manual identification, the data were not used in our analysis. Only the pairs of DSS and NIR objects, identified through the above fitting procedure, were regarded as the same objects.

3.1.6. The estimation of AGN variability

In order to derive the variability of AGNs from the difference between their magnitudes observed on different nights, it is necessary to determine the fiducial which should be subtracted from such difference. Let $\Delta m_i = m_{i,2} - m_{i,1}$ be the difference between the instrumental magnitudes of the i -th reference object observed on two different nights, and $\sigma_{\Delta m_i}^2 = \sigma_{m_{i,2}}^2 + \sigma_{m_{i,1}}^2$ its measurement errors, where i runs from 1 to N . The subscript 1 or 2 refers to the first or second measurement of the two observations, respectively.

The distribution of Δm_i is broader than expected from $\sigma_{\Delta m_i}$. This broadening likely stems from an error in the flat fielding which would equally affect all reference objects regardless of their luminosity. We incorporate this extra error σ_f in the estimation of the total error, so that the distribution of Δm_i conforms to χ^2 distribution. The value of σ_f is then obtained from solving the following equation:

$$\sum_i \frac{(\Delta m_i - \Delta m)^2}{\sigma_{\Delta m_i}^2 + \sigma_f^2} = N - 1 \quad , \quad (1)$$

where Δm is a weighted average given by

$$\Delta m = \sum_i \frac{\Delta m_i}{\sigma_{\Delta m_i}^2 + \sigma_f^2} / \sum_i \frac{1}{\sigma_{\Delta m_i}^2 + \sigma_f^2} \quad , \quad (2)$$

where we set $\sigma_f = 0$ if no real value exists. Substitution of the value of σ_f into equation 2 gives the value of Δm which should be used as a fiducial in deriving the variability of AGNs. The uncertainty of this fiducial is estimated as

$$\sigma_{\Delta m}^2 = \frac{1}{N - 1} \sum_i \frac{(\Delta m_i - \Delta m)^2}{\sigma_{\Delta m_i}^2 + \sigma_f^2} / \sum_i \frac{1}{\sigma_{\Delta m_i}^2 + \sigma_f^2} \quad . \quad (3)$$

The variability of AGN is therefore given by

$$\Delta m_{\text{AGN}} = m_{\text{AGN},2} - m_{\text{AGN},1} - \Delta m \quad , \quad (4)$$

and its error by

$$\sigma_{\Delta m_{\text{AGN}}}^2 = \sigma_{m_{\text{AGN},2}}^2 + \sigma_{m_{\text{AGN},1}}^2 + \sigma_{\Delta m}^2 \quad . \quad (5)$$

The process of determining the fiducial Δm is iterated, by excluding abnormal reference objects beyond a deviation of 5σ deviation. Three iterations suffice to exclude all such abnormal objects which are mostly either misidentifications, or near the edge of frame, or intrinsically variable stars. After convergence at 5σ , the iterative rejection is repeated at 3σ .

An example of differential photometry is shown in Fig. 1, where the difference $m_{\text{AGN},2} - m_{\text{AGN},1}$ for Mark 1320 in the H band is plotted at $i = 0$, together with Δm_i for five reference objects from $i = 1$ to 5. It is evident that the fiducial Δm (dashed horizontal line) yields $\Delta m_{\text{AGN}} = -0.55$ mag, that is, Mark 1320 was brightened by 0.55 mag.

3.2. The effect of PSF variability

The determined variability, Δm_{AGN} , of AGNs by differential photometry is less sensitive to PSF variation as compared to that by standards-based photometry. In principle, the effect of PSF variation on differential photometry is canceled out, if the PSFs of target and reference objects are of the same shape. However, since the target AGNs have more extended profiles than reference objects that are mostly stars, the effect of PSF variation is not completely canceled out. The variability of AGNs, corrected for the effect of PSF variation, is therefore given by

$$\Delta m_{\text{AGN}} = m_{\text{AGN},2} - m_{\text{AGN},1} - \Delta m - \Delta m_{\text{PSF}} \quad , \quad (6)$$

and its error by

$$\sigma_{\Delta m_{\text{AGN}}}^2 = \sigma_{m_{\text{AGN},2}}^2 + \sigma_{m_{\text{AGN},1}}^2 + \sigma_{\Delta m}^2 + \sigma_{\Delta \text{PSF}}^2 \quad . \quad (7)$$

We characterize the PSFs of the reference objects by their FWHMs measured with the `cl` script in the IRAF `imexamine` task. There is a tendency for the FWHMs from the IRAF output to be larger for fainter objects. In order to avoid this tendency, we use only the reference objects for which photon counts at their profile center exceed 50. We estimate

the difference $\Delta\text{FWHM}_i = \text{FWHM}_{i,2} - \text{FWHM}_{i,1}$ for the i -th reference object around the target AGN, where the subscript 1 or 2 refers to the first or second measurement from the two observations, respectively. We then derive the correction $\Delta m_{\text{PSF},i}$ due to an intrinsic nonzero ΔFWHM_i , by convolving the smaller- FWHM_i image to match the larger- FWHM_i image. This analysis was performed using the IRAF `gaus` task, and the correction $\Delta m_{\text{PSF},i}$ is derived as a function of ΔFWHM_i . Taking an average over all the reference objects around the target AGN, we obtain Δm_{PSF} and ΔFWHM , which will be used to correct Δm_{AGN} for the effect of a nonzero intrinsic PSF.

The top panel of Fig. 2 shows the correction Δm_{PSF} plotted against ΔFWHM , based on the data for which the accuracy of instrumental magnitude is better than 0.02 mag. It is clear that the better (poorer) seeing in the later of two observations gives fake darkening (brightening) in Δm_{AGN} . The plots in this panel are fitted by a linear relation between Δm_{PSF} and ΔFWHM , and the dispersion around Δm_{PSF} is expressed, in terms of ΔFWHM , as

$$\sigma_{\Delta m_{\text{PSF}}}^2 = \left(\frac{d\Delta m_{\text{PSF}}}{d\Delta\text{FWHM}} \right)^2 \sigma_{\Delta\text{FWHM}}^2 . \quad (8)$$

The bottom panel shows the frequency distribution of Δm_{PSF} . Since the data are restricted to brighter AGNs of high accuracy, we cannot individually correct the variability of AGNs in our sample. With this restriction, we rather estimate $\Delta m_{\text{PSF}} \approx 0$ and $\sigma_{\Delta m_{\text{PSF}}} \approx 0.01$ from the combined JHK' data and substitute these values in equations 6 and 7, irrespective of the passband.

Here, the estimate of Δm_{PSF} has been limited to bright AGNs only. However, contrary to the case of bright AGNs, the fake variability due to PSF variation would be even smaller for fainter AGNs, because only the central, point-like part of their profiles is visible with their extended hosts mostly below detection. Therefore, the estimate of $\Delta m_{\text{PSF}} \approx 0$ from bright AGNs is also used to correct the variability of fainter AGNs in this paper.

It is worth mentioning that this paper is a preliminary study for a monitoring program, MAGNUM, which is expected to go fainter ($R_{lim} \sim 23\text{mag}$) and more accurately ($\sigma \sim 0.01\text{mag}$), compared with our observations here. In such a program, the correction factor for each of AGNs is obtained as a function of varying luminosity and PSF in the course of long-term monitoring observations, and the method of convolving obtained images, as used here, may not be necessary.

3.3. The test of the error estimation

Error estimation in the variability data is very important. When the error is sufficiently small, a fake variability originates from only the dispersion of the photometric data. On the other hand, when the error is too large, the significance of any detected variability cannot be certain.

The variability of reference objects was fairly small, because most of them are stars. Their corrected variability is denoted by $\Delta m_{c,i} = \Delta m_i - \Delta m$, and the corrected error is calculated by $\sigma_{\Delta m_{c,i}}(\text{cal})^2 = \sigma_{\Delta m_i}^2 + \sigma_f^2$. We divide the reference objects into subsamples according to their calculated errors binned at intervals of 0.01. For the subsample in each error bin, we have constructed the frequency distribution of corrected variability, and derived the median Δm_c and dispersion $\sigma_{\Delta m_c}(\text{dsp})$ for a sample in each error bin centered at $\sigma_{\Delta m_c}(\text{cal})$.

Figure 3 shows Δm_c and $\sigma_{\Delta m_c}(\text{dsp})$ plotted against $\sigma_{\Delta m_c}(\text{cal})$ in the J , H , and K' bands. It is seen from this figure that the $\sigma_{\Delta m_c}(\text{cal})$'s are nearly equal to the $\sigma_{\Delta m_c}(\text{dsp})$'s, but are mostly below the dotted line of $\sigma_{\Delta m_c}(\text{cal}) = \sigma_{\Delta m_c}(\text{dsp})$. This indicates a slight overestimation of $\sigma_{\Delta m_c}(\text{cal})$, which is desirable rather than the converse, so that our error estimation of differential photometry is quantitatively reliable over a range of error from

0.01 up to 0.1 for the J , H and K' bands. The medians, Δm_c 's, are almost equal to zero.

3.4. A comparison of the accuracies of two photometry methods

In this paper we have used a method of differential photometry to detect the NIR variability of AGNs. On the other hand, however, we can also use a method of standards-based photometry to detect AGN variability in our sample. In this section we compare the accuracies of these two methods when applied to the same AGNs.

The differential photometry uses the instrumental, aperture magnitudes with a fixed aperture of $r = 3$ pixels, while the standards-based photometry uses aperture magnitudes with $r = 7, 10, 12$ and 15 pixels. By standards-based photometry we obtained a pair of magnitude and measurement error for each object observed on two different nights, and determined the magnitude difference $\Delta m_i = m_{i,2} - m_{i,1}$ and its error $\sigma_{\Delta m_i}^2 = \sigma_{m_{i,2}}^2 + \sigma_{m_{i,1}}^2$. The analysis below is limited to the data for which more than two reference objects were used for differential photometry.

Figure 4 shows the comparison between the variabilities of AGNs by differential photometry $\Delta m_{\text{AGN}}(\text{dif})$ and by standards-based photometry $\Delta m_{\text{AGN}}(\text{std})$ for the case of the J band. Similar results in the H and K' bands are not shown here. The distribution of data points, for the standards-based photometry with $r = 7$ pixels, is elongated, more or less, along the diagonal in the $\Delta m_{\text{AGN}}(\text{dif})$ versus $\Delta m_{\text{AGN}}(\text{std})$ diagram. However, increasing the aperture from $r = 7$ to 15 pixels steadily increases the error (see below), which destroys a clear correlation between $\Delta m_{\text{AGN}}(\text{dif})$ and $\Delta m_{\text{AGN}}(\text{std})$.

Figure 5 shows the comparison between errors by differential photometry $\sigma_{\Delta m_{\text{AGN}}}(\text{dif})$ and by standards-based photometry $\sigma_{\Delta m_{\text{AGN}}}(\text{std})$ for the case of J band. Similar results in the H and K' bands are not shown here. The first feature to be noticed is that

many data points are concentrated along a linear sequence in the $\sigma_{\Delta m_{\text{AGN}}}(\text{dif})$ versus $\sigma_{\Delta m_{\text{AGN}}}(\text{std})$ diagram. The second feature is that the sequence is inclined much closer to the $\sigma_{\Delta m_{\text{AGN}}}(\text{std})$ -axis for larger aperture. These features are consistent with a tendency in aperture photometry such that the S/N ratio becomes smaller for larger aperture, enhancing $\sigma_{\Delta m_{\text{AGN}}}(\text{std})$.

The linear sequence seen in the $\sigma_{\Delta m_{\text{AGN}}}(\text{dif})$ versus $\sigma_{\Delta m_{\text{AGN}}}(\text{std})$ diagram always has a slope much less than 1. In particular, the slope is about 0.5 for the aperture of $r = 7$ pixels, and about 0.1 for $r = 15$ pixels. This shows that the accuracy of differential photometry is superior to standards-based photometry.

A small number of outliers exist far above the linear sequence. Their existence may be explained partly by larger fiducial error in differential photometry which gives a larger $\sigma_{\Delta m_{\text{AGN}}}(\text{dif})$ even for higher S/N ratio. Such fiducial error may stem from a possible error of flat fielding, a contamination by variable stars in reference objects, and inaccurate photometry of objects near the edge of the frame. Because of their small number, exclusion of such outliers from the sample does not improve the statistics in this paper.

Next, we quantitatively compare the accuracies of two methods, based on a frequency distribution of AGNs with respect to an error ratio $c = \sigma_{\Delta m_{\text{AGN}}}(\text{std})/\sigma_{\Delta m_{\text{AGN}}}(\text{dif})$. Here the data plotted in Fig. 5 are used. Let $f(\geq c)$ be a fractional number of AGNs, having an error ratio larger than c , relative to their total number. Figure 6 shows the fraction $f(\geq c)$ plotted as a function of aperture for various values of c in the J , H , and K' bands.

This figure indicates that for most cases the fractional number of AGNs with the error ratio beyond unity comprises about $f = 80\%$ in the sample. For standards-based photometry, the aperture which is 3 or 4 times larger than typical FWHM is usually used to avoid the influence of PSF variation. This corresponds to an aperture of $r = 10$ or 12 pixels, because a typical FWHM is about 3 pixels in our observations. Such apertures

give $c \approx 2 - 3$ for $f = 50\%$, as seen from Fig. 6. Therefore, the accuracy of differential photometry is 2 – 3 times higher than that of standards-based photometry.

Further suppression of fiducial error in differential photometry is possible, if the effects of flat-fielding error and inaccurate photometry near the frame edge can be minimized. It is then hoped that many bright reference objects can be chosen close enough to the target AGN, but not too close to produce confusion. In such an ideal situation, the photometry only in some relevant area of all the dithering frames suffices, in contrast to the photometry over the entire dithered area as used in this paper.

In order for the MAGNUM Project to realize much higher accuracy in differential photometry, we select the candidate AGNs, which should satisfy the above criterion. Owing not only to the sample selection, but also considering exposure time and dithering pattern, we can make the analysis go fainter without degrading the S/N ratio.

4. Results

A certain fraction of AGNs have certainly varied in the J , H and K' bands. In this paper, we consider a sample of 226 AGNs data obtained with more than two reference objects and with an accuracy better than 0.1 mag. Their variability data are tabulated in Table 1. We show the distribution of variability Δm_{AGN} and redshift z for the entire sample in Fig. 7, and the histogram with respect to Δm_{AGN} in Fig. 8.

As a measure of this variability, we introduce a ratio $R = \Delta m_{\text{AGN}}/\sigma_{\Delta m_{\text{AGN}}}$, and construct the frequency distribution of AGNs with respect to R . Figure 9 shows such a frequency distribution for our entire sample of 226 AGNs, and two samples of radio-quiet and radio-loud AGNs. All AGNs with $R > 5$ are those that have varied most certainly and are included in the rightmost bin of $R = 5 - 6$. For both the entire sample and radio-quiet

sample, the frequency monotonically decreases rightwards from the bin of $R = 0 - 1$ to $R = 4 - 5$, and the peak occurs in the rightmost bin of $R = 5 - 6$. However, because of the small sample size, it is not easy to see similar features for the radio-loud sample. These results hold commonly for the J , H and K' bands.

Figure 10 shows the frequency distribution for the radio-quiet and radio-loud AGNs which are furthermore classified by rest-frame time interval Δt_{rest} between our two observations made for each AGN. For the radio-quiet AGNs with short time interval of $\Delta t_{\text{rest}} = 100 - 400$ days, the frequency monotonically decreases with increasing R , and the frequency for $R > 5$ is rare. On the other hand, for the radio-quiet AGNs, with the long time interval of $\Delta t_{\text{rest}} = 400 - 800$ days, the frequency stays almost constant over a range of $R = 0 - 5$, and shows a prominent peak at $R > 5$. Therefore, most of radio-quiet AGNs that have certainly varied are those with time interval exceeding 400 days in rest frame. For the radio-loud AGNs, the frequency stays, more or less, constant, independent of time interval, though the sample size is too small to claim it definitely.

Figure 11 shows the frequency distribution for all AGNs which are divided by their error into three groups of high accuracy of $\sigma_{\Delta m_{\text{AGN}}} < 0.03$, intermediate accuracy of $\sigma_{\Delta m_{\text{AGN}}} = 0.03 - 0.05$, and low accuracy of $\sigma_{\Delta m_{\text{AGN}}} = 0.05 - 0.1$. It is seen from this figure that the frequency distributions for these three groups differ remarkably from each other. For the high-accuracy group, the frequency is localized in the rightmost bin of $R > 5$, indicating that most AGNs in this group have certainly varied. On the other hand, for the low-accuracy group, the frequency is enhanced on the left. The frequency distribution for the intermediate-accuracy group is in between these two extremes.

Table 2 tabulates the estimated fraction of AGNs that have certainly varied with 2σ or 3σ confidence in various cases of different samples. The fraction of varied AGNs with 2σ confidence in the high-accuracy group is 85%(J), 82%(H), and 73%(K'), and the fraction

for 3σ confidence is 73%(J), 67%(H), and 65%(K'). Therefore, based on the high-accuracy group with $\sigma_{\Delta m_{\text{AGN}}} < 0.03$, we at least conclude that the detection rate of variable AGNs is about 80%(2σ) or 68%(3σ).

If the sample indeed contains some non-variable AGNs, the fraction of variable AGNs should become saturated as the accuracy increases. Comparing three accuracy groups, we see no sign of such saturation towards higher accuracy. However, it is not possible to extrapolate this tendency arriving eventually at 100% to much higher accuracy, because other parameters are not uniform in the three accuracy groups. In particular, the high-accuracy group is biased in favor of nearby, bright, and radio-quiet AGNs.

In contrast with our higher detection rate, Neugebauer et al. (1989) reported that about 24% of 108 AGNs in their K -band monitoring sample have certainly varied at the 99.7% confidence level, which is comparable to our result based on the low-accuracy group with $\sigma_{\Delta m_{\text{AGN}}} = 0.05 - 0.1$. Moreover, the shape of frequency distribution with respect to R by Neugebauer et al. (1989) is also consistent with our result based on the low-accuracy group. Consequently, it is likely that their low detection rate is only apparent because of the rather low accuracy in their observations which were based on the single detector with a 5 – 15 arcsec beam.

5. Conclusion

We present the JHK' variability data for a sample of 226 AGNs consisting mainly of Seyfert 1 AGNs and QSOs, each of which was observed twice in the period of 1996 – 1998 in time interval of a year or more separating the observations. About a quarter of the AGNs in each category are radio loud. The AGNs were selected covering a wide range of redshift from $z = 0$ to 1, and of absolute B -magnitude from $M_B = -30$ mag to -20 mag.

The effect of PSF variation cannot be canceled completely in the differential photometry, because the target AGNs are not always seen as having the same PSF profiles as the surrounding reference objects. The systematic error arising from this PSF effect is estimated as about 0.01mag, which is smaller than other errors. Considering all systematic errors from different sources, we were able to use a small aperture of 3 pixels, comparable to the seeing size. As a result, smaller statistical error was realized in the determination of AGN variability by differential photometry than by usual standards-based photometry. In order to check the accuracy of our result, we also applied the differential photometry to the reference objects around AGNs, and confirmed that the above error estimation was reasonable, independent of the passband.

Significance of AGN variability was measured by a ratio of variability relative to estimated error $R = \Delta m_{\text{AGN}} / \sigma_{\Delta m_{\text{AGN}}}$. Since the R -values of the AGNs in our sample are similarly distributed irrespective of passband, we average the JHK' variability for the AGNs of $\sigma_{\Delta m_{\text{AGN}}} < 0.1$ mag. Then, the rate of variability detection, or the fraction of certainly varied AGNs in this sample is 58%(2 σ) or 44%(3 σ).

We furthermore divide the sample into three groups of different error ranges such as high accuracy of $\sigma_{\Delta m_{\text{AGN}}} < 0.03$, intermediate accuracy of $\sigma_{\Delta m_{\text{AGN}}} = 0.03 - 0.05$, and low accuracy of $\sigma_{\Delta m_{\text{AGN}}} = 0.05 - 0.1$. We then estimate the rate of variability detection in each of three groups. The frequency distribution of the AGNs with respect to R for the low-accuracy group was skewed towards smaller R . On the other hand, for the high-accuracy group, the frequency distribution shows a prominent peak at $R > 5$, and the fraction of certainly varied AGNs in this group is 80%(2 σ) or 68%(3 σ). Thus, the rate of variability detection is larger for higher accuracy. Since this tendency shows no saturation, it does not exclude the possibility that all AGNs are indeed variable.

In conclusion, the high detection rate in this paper is mainly obtained by our use of

differential photometry with a small aperture of 3 pixels. The advantage of using differential photometry is to enable an efficient detection of variability in as many AGNs as possible with observations made only twice, with a long time interval of a year or more separating the observations. Furthermore, the advantage of using a small aperture is not only to improve the S/N ratio but also to decrease the contribution of the AGN host galaxy within the aperture, especially for nearby AGNs.

We are grateful to H. Okuda, M. Narita and other staff of the infrared astronomy group of the Institute of Space and Astronautical Science (ISAS) for their support in using their 1.3m telescope. We thank the staff of the Advanced Technology Center of the National Astronomical Observatory of Japan (NAOJ) for their new coating of the primary mirror of the 1.3m telescope at the ISAS. Gratitude is also extended to the Computer Data Analysis Center of the NAOJ. This work has made use of the NASA/IPAC Extra Galactic Database (NED), and has been supported partly by the Grand-in-Aid (07CE2002, 10304014) of the Ministry of Education, Science, Culture, and Sports of Japan and by the Torey Science Foundation.

REFERENCES

- Barvanis,R., 1992, ApJ, 400, 502
- Borgeest, U., and Schramm, K.-J. 1994, A&A, 284, 764
- Clavel, J., Wamsteker, W., and Glass, I. S. 1989, ApJ, 1989, 236
- Giveon, U., Maoz, D., Kaspi, S., Netzer, H., and Smith, P. S. 1999, MNRAS, 306, 637
- Kobayashi, Y., Yoshii, Y., Peterson, Bruce A., Miyazaki, S., Aoki, T., Minezaki, T., Kawara, K., Enya, K., Okada, N., Suganuma, M., Greene, B., O'Brien, M., Randall, and Lawrence K. 1998, Proc. SPIE Vol. 3352, p. 120-128, Advanced Technology Optical/IR Telescopes VI, Larry M. Stepp, Ed.
- Kobayashi, Y., Yoshii, Y., Peterson, Bruce A., Minezaki, T., Enya, K., Suganuma, M., and Yamamuro, T. 1998, Proc. SPIE Vol. 3354, p. 769-776, Infrared Astronomical Instrumentation, Albert M.Fowler, Ed.
- Kobayashi, Y., Fang, G., Minezaki, T., Waseda, K., Nakamura, K., and Sato, S. 1994, Proc. SPIE Vol. 2198, p. 603-613, Instrumentation in Astronomy VIII, David L. Crawford, Eric R. Craine, Eds.
- Netzer, H., Heller, A., Loinger, F., Alexander, T., Baldwin, J. A., Wills, B. J., Han, M., Frueh, M., and Higdon, J. L. 1996, MNRAS, 279, 429
- Neugebauer, G., Soifer, B. T., Matthews, K., and Elias, J. H. 1989, AJ, 97, 957
- Veron-Cetty, M.-P., and Veron, P. 1998, A Catalogue of quasars and active nuclei, Edition: 8th ed., Publisher: Garching: European Southern Observatory (ESO), 1998, Series: ESO Scientific Report Series vol no: 18
- Veron-Cetty, M.-P., and Veron, P. ESO Scientific Report, Garching: European Southern Observatory (ESO), 1993, 6th ed.

Veron-Cetty, M.-P., and Veron, P. ESO Scientific Report, Garching: European Southern Observatory (ESO), 1996, 7th ed.

Fig. 1.— An example of measuring the AGN variability by differential photometry. Shown are the differences of two H -magnitudes measured on 96/02/11 and 97/12/27 for Mark 1320 ($i = 0$) and its nearby reference objects ($i = 1$ to 5). Mark 1320 has brightened by 0.55 mag, relative to the fiducial (dashed line) defined by the reference objects.

Fig. 2.— The magnitude correction, Δm_{PSF} , for the effect of PSF variation in the estimation of AGN variability, based on the data for which the magnitude accuracy is less than 0.02 mag. *Top panel:* The relation between the correction, Δm_{PSF} , and the difference of the FWHMs measured on two different nights, ΔFWHM . *Bottom panel:* The histogram of Δm_{PSF} .

Fig. 3.— The median of corrected variability, Δm_c , and its dispersion, $\sigma_{\Delta m_c}(\text{dsp})$, for reference objects as a function of calculated error, $\sigma_{\Delta m_c}(\text{cal})$. Triangles, squares, and circles represent the J , H , and K' bands, respectively. The filled symbols are for Δm_c , and the open symbols are for $\sigma_{\Delta m_c}(\text{dsp})$.

Fig. 4.— A comparison between AGN variabilities determined by differential photometry, $\Delta m_{\text{AGN}}(\text{dif})$, and standards-based photometry, $\Delta m_{\text{AGN}}(\text{std})$. Shown are the J -band results for various apertures of 7, 10, 12, and 15 pixels.

Fig. 5.— A comparison between errors of AGN variabilities determined by differential photometry, $\sigma_{\Delta m_{\text{AGN}}}(\text{dif})$, and standards-based photometry, $\sigma_{\Delta m_{\text{AGN}}}(\text{std})$. Shown are the J -band results for various apertures of 7, 10, 12, and 15 pixels.

Fig. 6.— The fractional number of AGNs, $f(\geq c)$, as a function of aperture for various values of error ratio defined by $c = \sigma_{\Delta m_{\text{AGN}}}(\text{std})/\sigma_{\Delta m_{\text{AGN}}}(\text{dif})$. The top, middle, and bottom panels are for the J , H , and K' bands, respectively.

Fig. 7.— The distribution of AGN variability, Δm_{AGN} , and redshift z , based on the data with more than two reference objects and with an accuracy higher than 0.1 mag. The top,

middle, and bottom panels are for the J , H , and K' bands, respectively.

Fig. 8.— The frequency distribution of variability, Δm_{AGN} , based on the data with more than two reference objects and with an accuracy higher than 0.1 mag.

Fig. 9.— The frequency distribution of AGNs having varied with respect to the ratio of $R = \Delta m_{\text{AGN}}/\sigma_{\Delta m_{\text{AGN}}}$. The top, middle, and bottom panels are for all AGNs, radio-quiet AGNs, and radio-loud AGNs, respectively.

Fig. 10.— The frequency distribution of AGNs having varied with respect to the ratio of $R = \Delta m_{\text{AGN}}/\sigma_{\Delta m_{\text{AGN}}}$. Same as in Fig. 9, but for radio-quiet AGNs (left column) and radio-loud AGNs (right column) subdivided by the rest-frame time interval, Δt_{rest} , between observations.

Fig. 11.— The frequency distribution of AGNs having varied with respect to the ratio of $R = \Delta m_{\text{AGN}}/\sigma_{\Delta m_{\text{AGN}}}$. Same as in Fig. 9, but for all AGNs subdivided by their variability error, $\sigma_{\Delta m_{\text{AGN}}}$.

Figure 1.

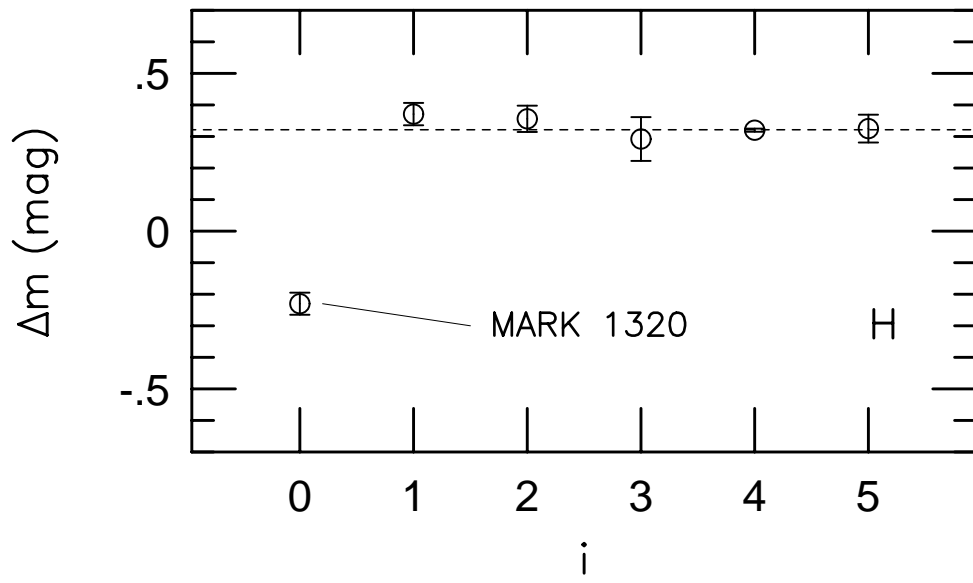


Figure 2.

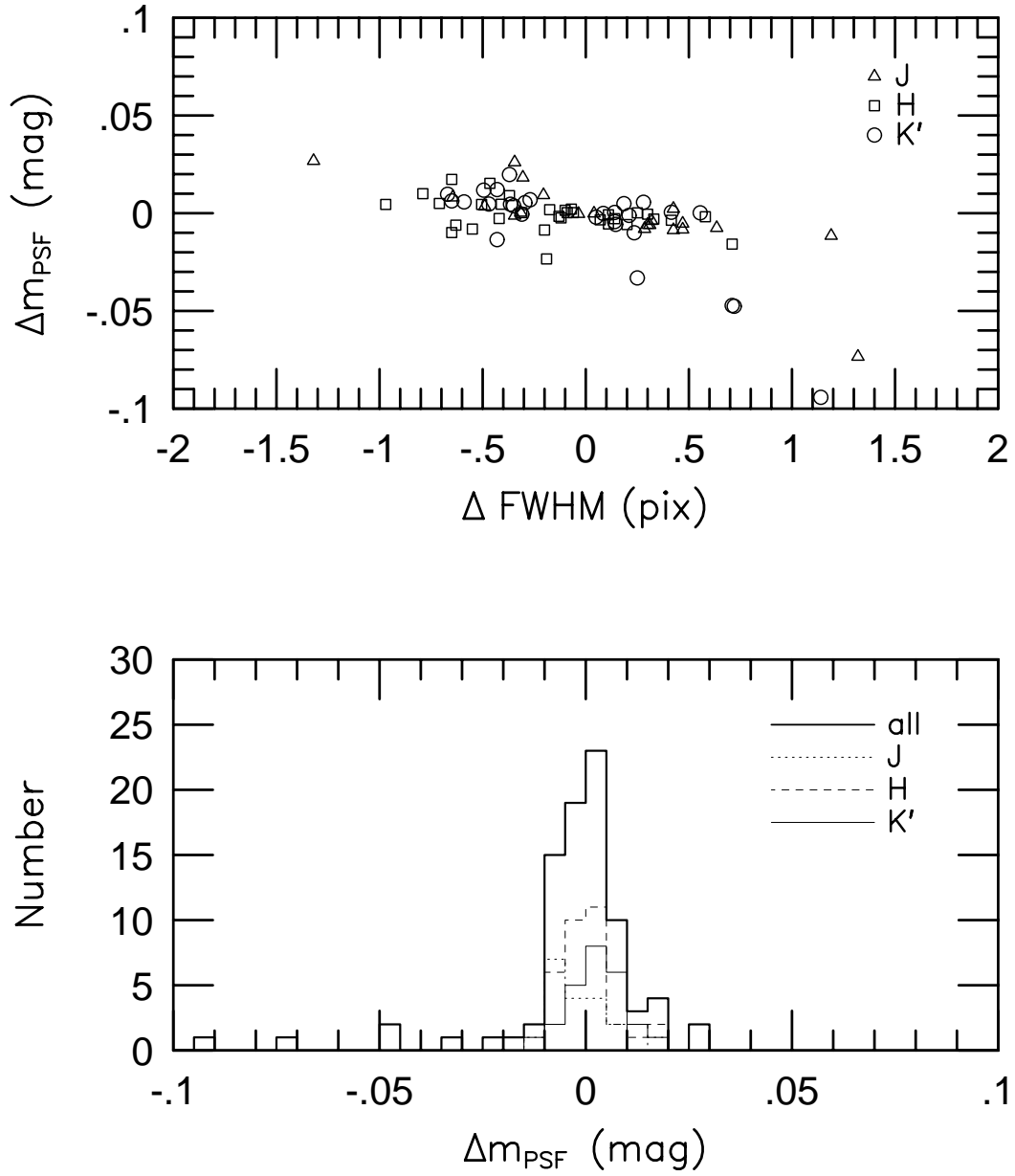


Figure 3.

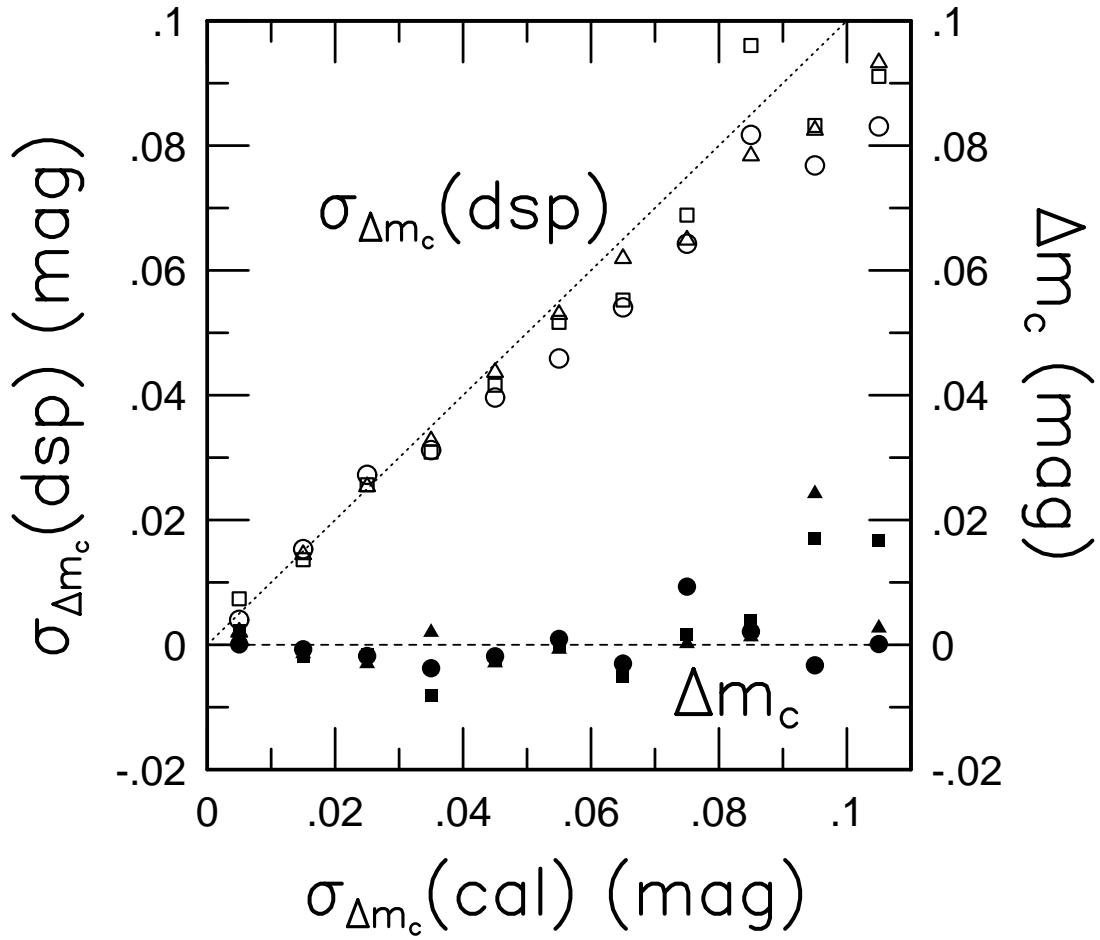


Figure 4.

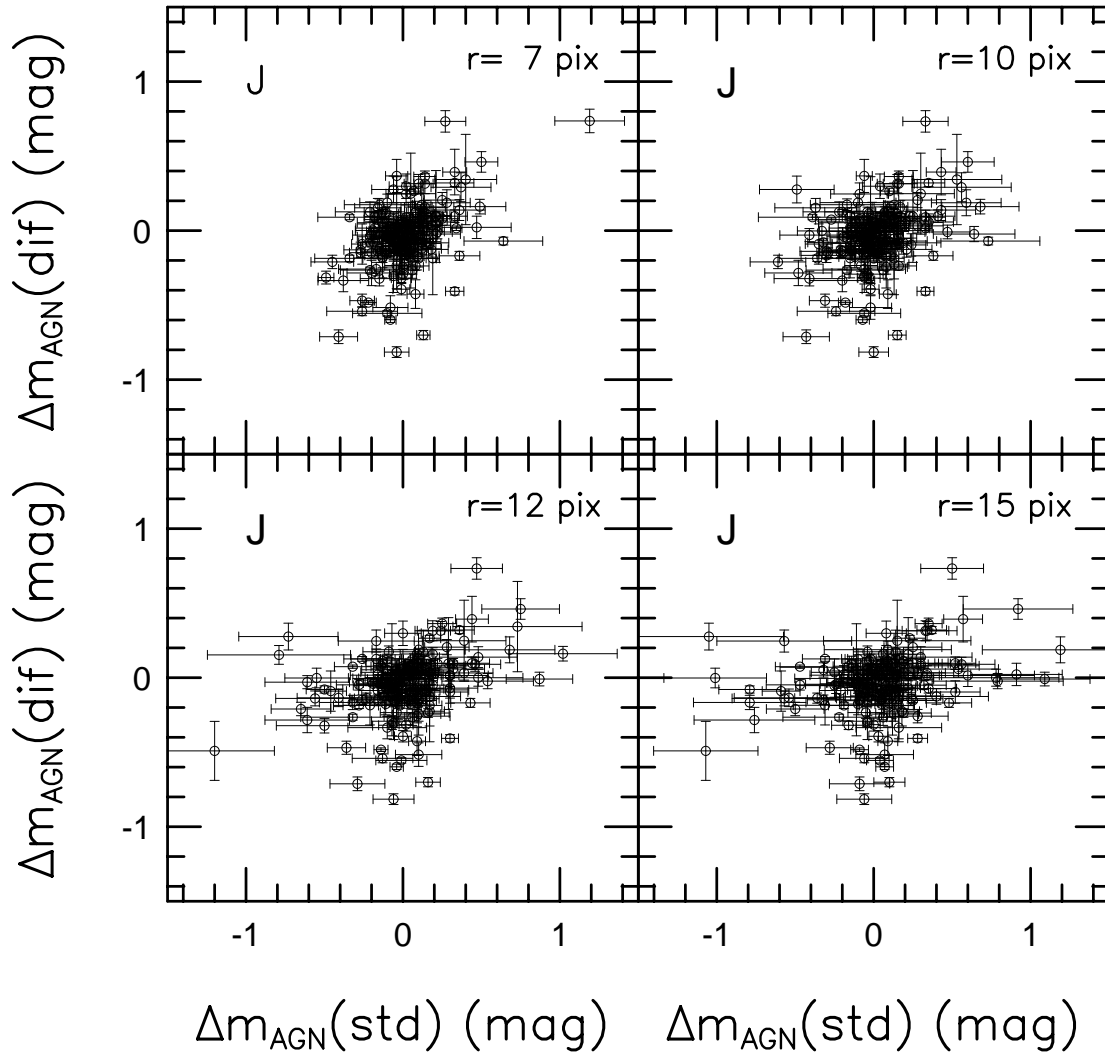


Figure 5.

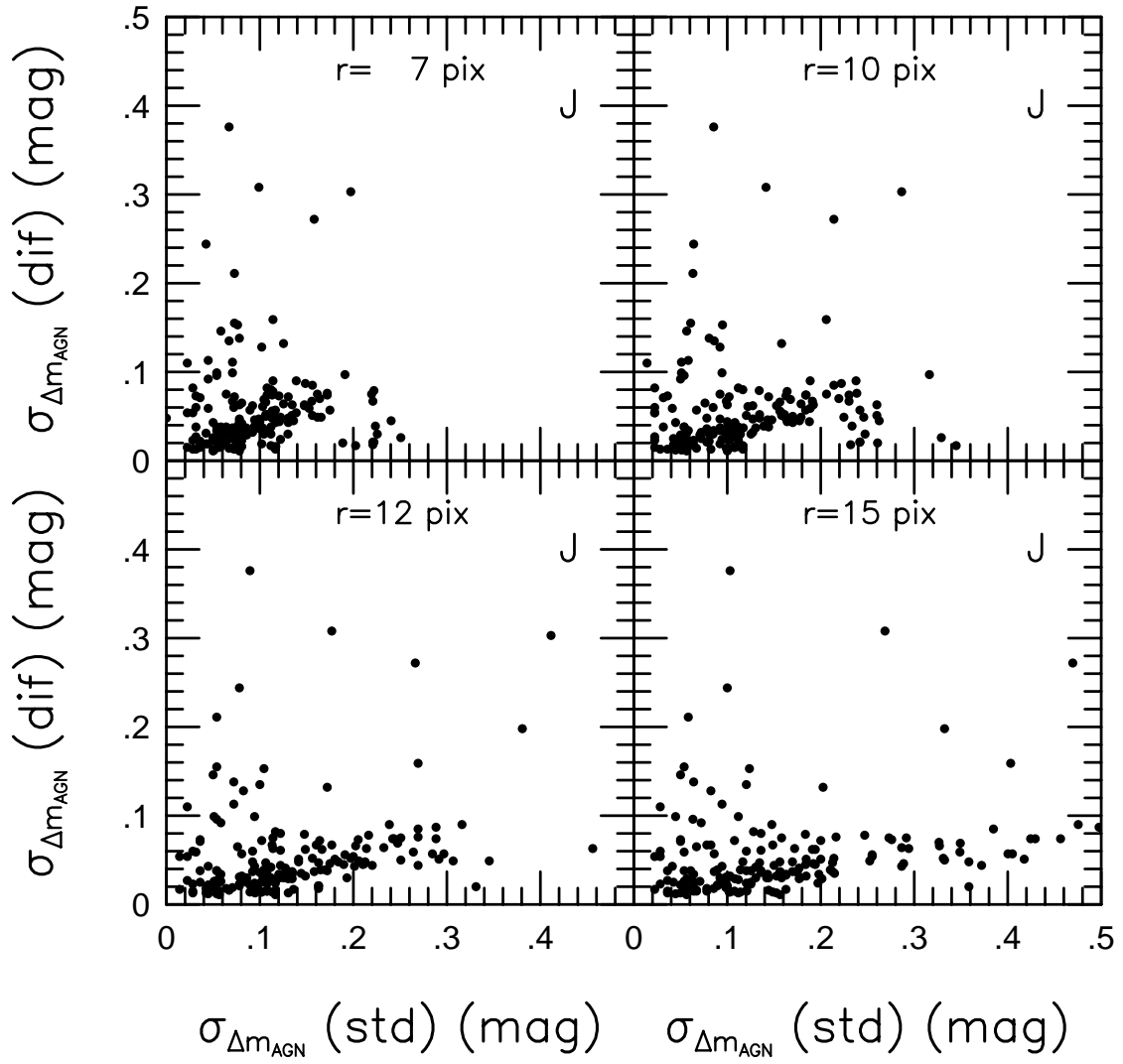


Figure 6.

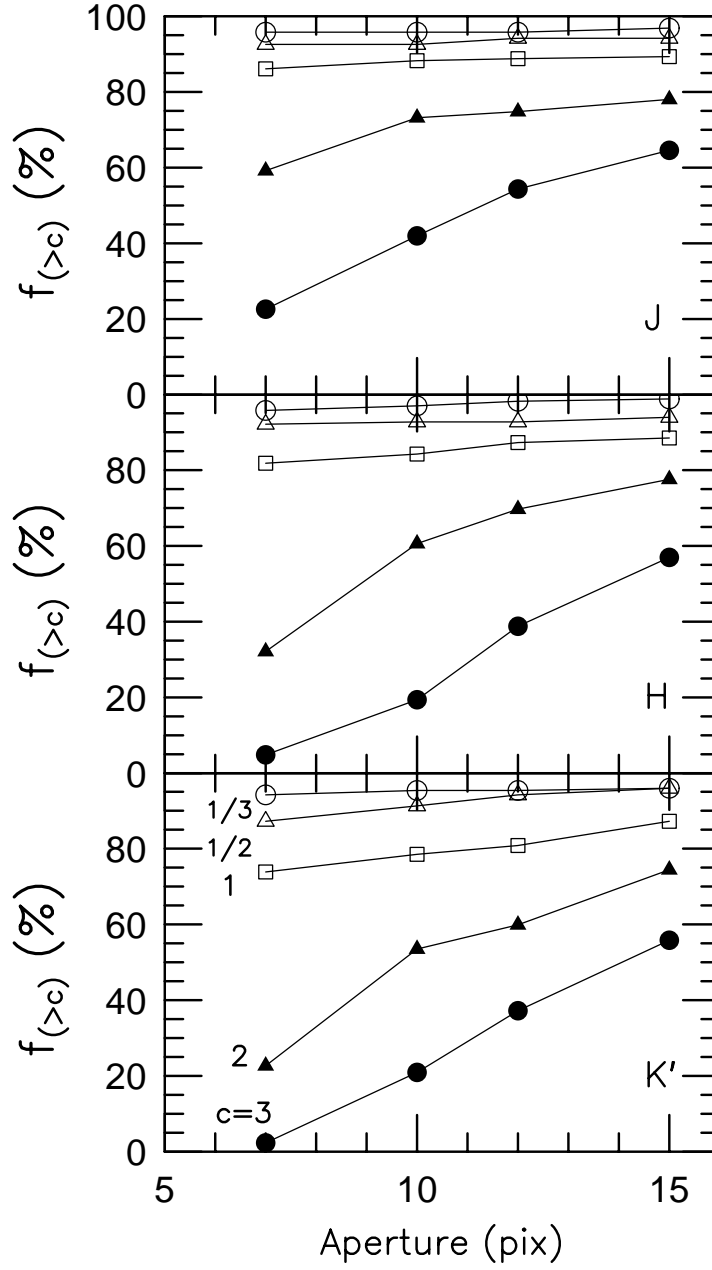


Figure 7.

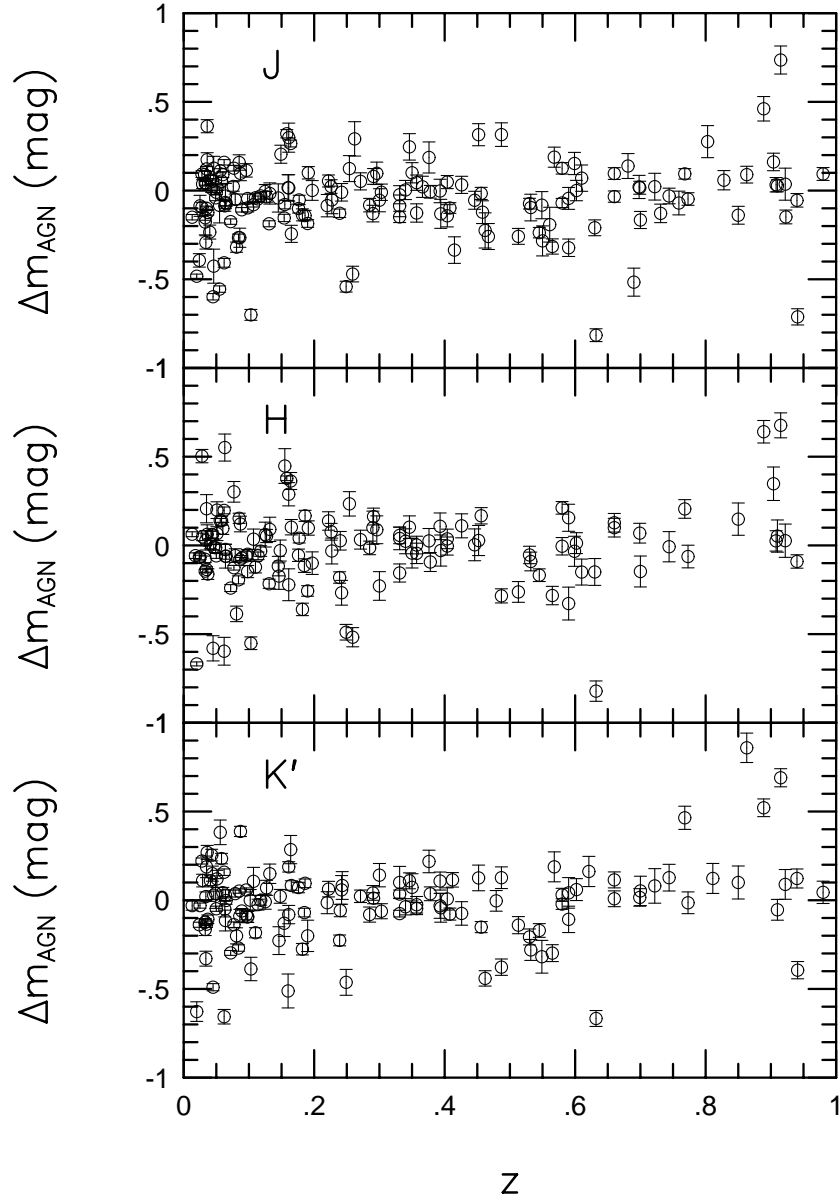


Figure 8.

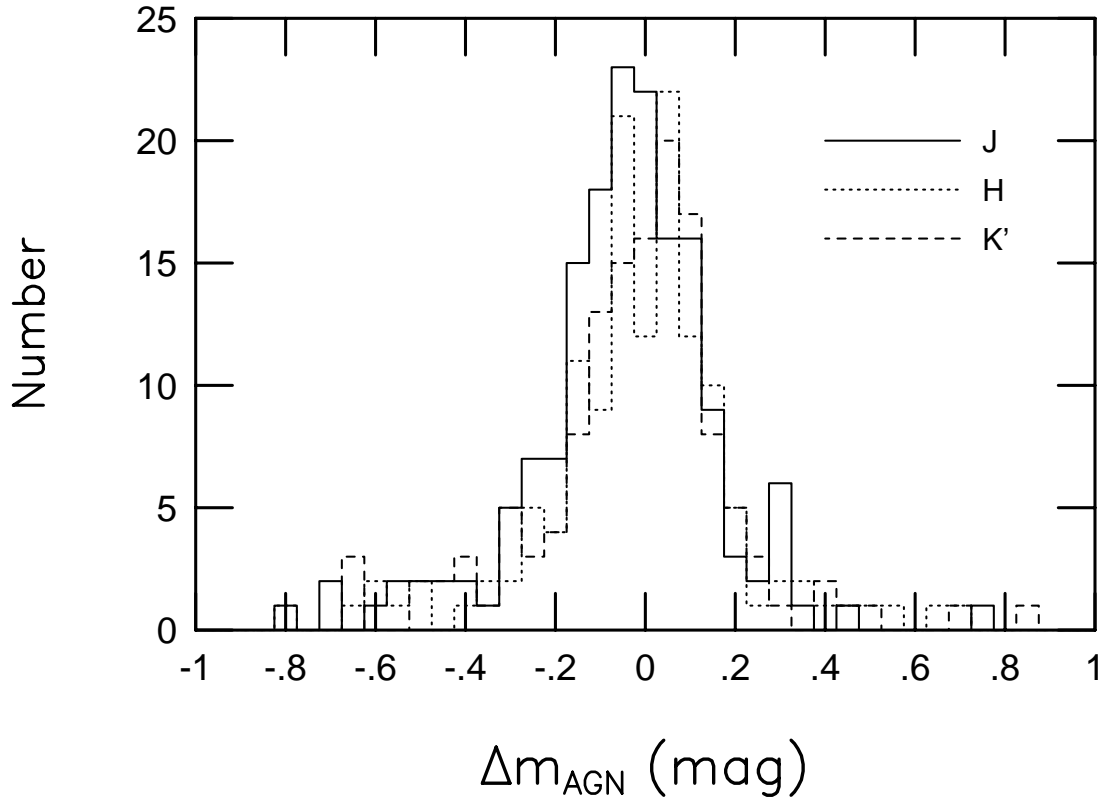


Figure 9.

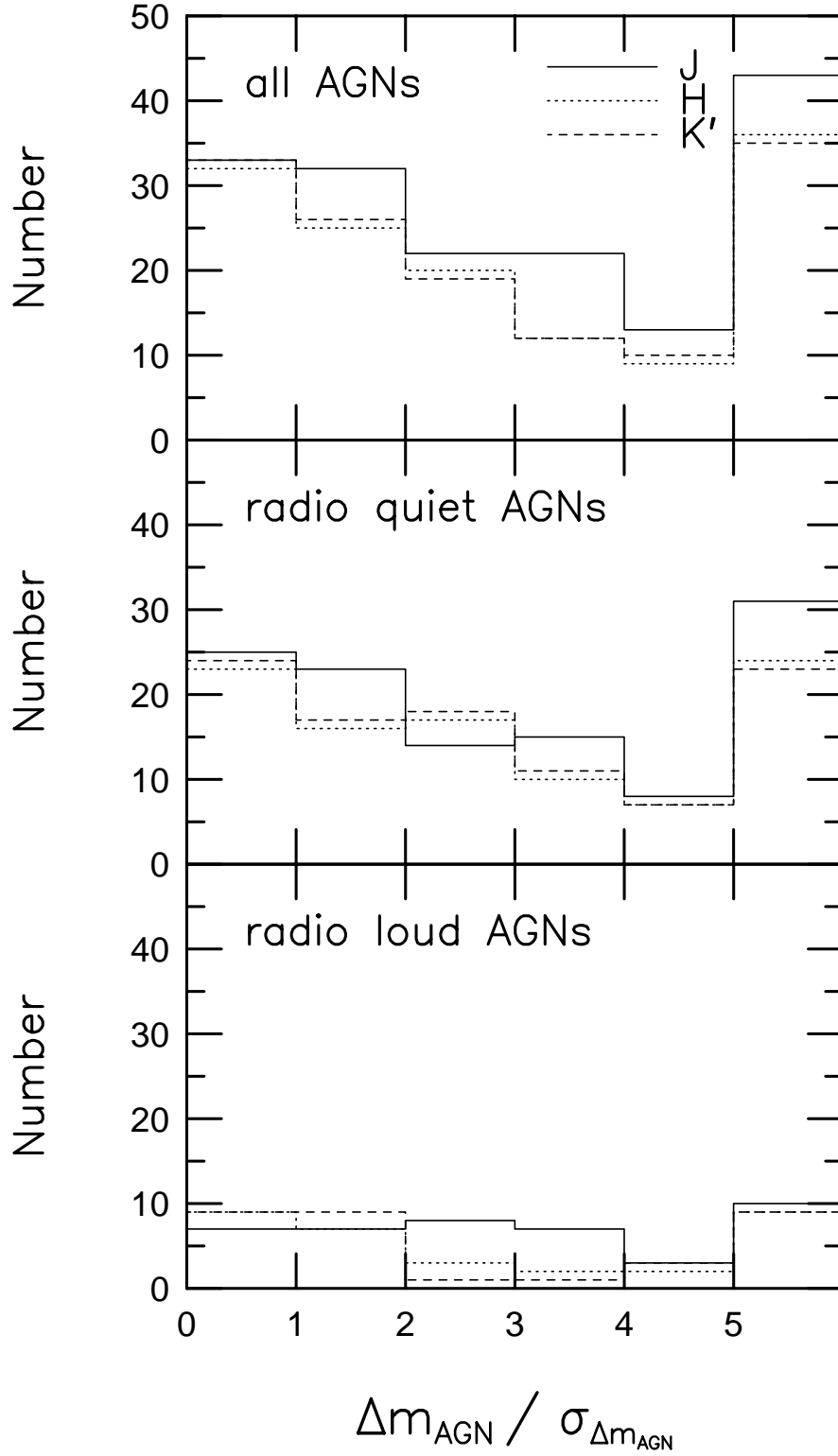


Figure 10.

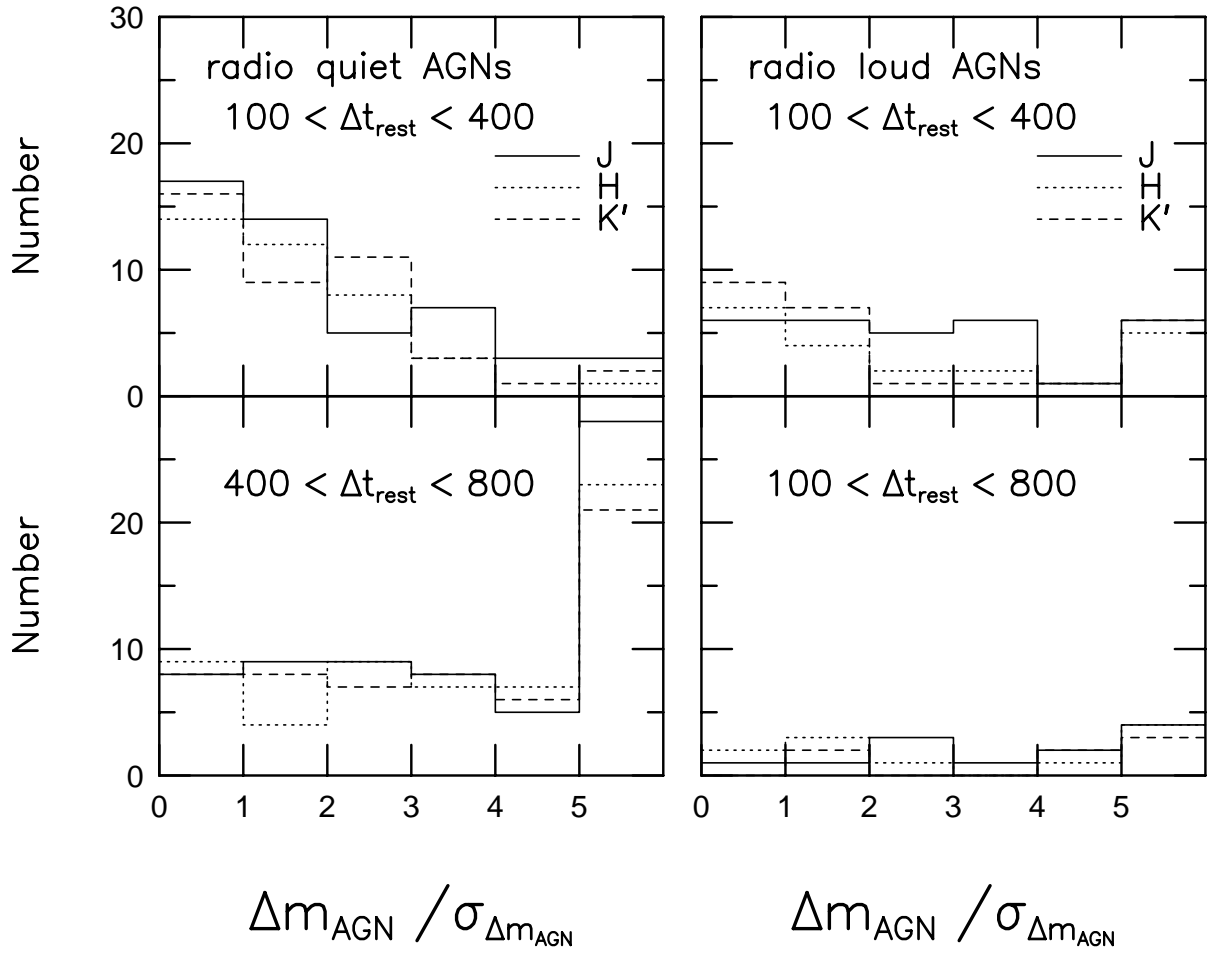


Figure 11.

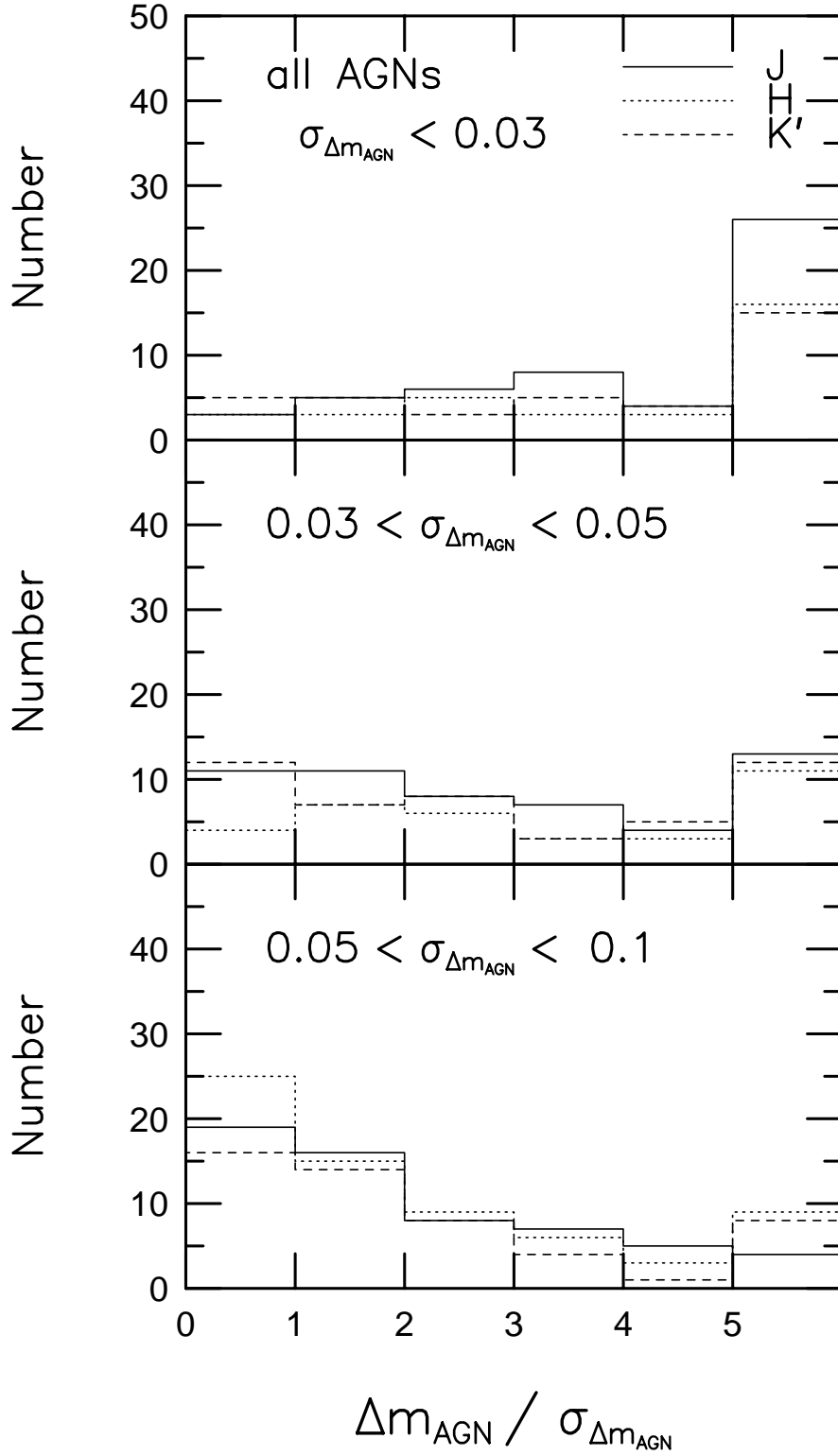


Table 1. Variability data of 226 AGNs

Number	Name	ΔJ	$\sigma_{\Delta J}$	n_J	ΔH	$\sigma_{\Delta H}$	n_H	$\Delta K'$	$\sigma_{\Delta K'}$	$n_{K'}$	date1	date2
1	PB 5669	–	–	–	0.366	0.126	6	-0.004	0.058	6	96/12/03	98/01/05
5	PB 5853	0.017	0.073	5	–	–	–	-0.511	0.096	8	96/12/03	98/01/21
7	PB 5932	0.048	0.037	10	0.037	0.055	5	0.162	0.105	9	96/12/01	98/01/26
8	MS 00377-0156	0.097	0.063	2	0.088	0.078	8	–	–	–	96/12/03	98/01/06
14	PKS 0130+24	0.315	0.062	11	0.028	0.085	10	0.126	0.072	9	96/12/01	98/01/21
15	UM 341	-0.030	0.082	1	–	–	–	0.031	0.076	1	96/12/01	97/12/27
19	KUV 01507-0744	-0.054	0.065	3	-0.229	0.081	3	0.141	0.066	2	96/11/25	97/12/31
20	PHL 1226	-0.142	0.063	5	-0.004	0.051	4	0.007	0.063	6	96/12/01	98/01/16
21	UM 381	0.027	0.034	3	0.053	0.091	3	-0.054	0.059	4	96/12/08	98/01/04
22	UM 153	0.096	0.033	9	0.100	0.053	9	0.115	0.045	7	96/12/08	98/01/05
23	MARK 1018	0.011	0.022	7	0.061	0.019	5	0.254	0.033	2	96/02/11	98/01/05
24	RXS J02070+2930	-0.041	0.023	7	-0.122	0.033	5	-0.183	0.029	5	96/02/11	98/01/05
25	MARK 586	-0.079	0.024	8	0.448	0.098	6	0.000	0.204	6	96/02/07	98/01/05
26	PKS 0214+10	-0.098	0.030	6	-0.072	0.108	8	-0.078	0.034	7	96/12/08	97/12/27
27	PB 9130	0.544	0.100	1	0.126	0.102	2	0.062	0.106	1	96/11/25	96/12/01
28	B3 0219+443	-0.139	0.050	26	0.148	0.091	21	0.100	0.093	13	96/12/22	98/01/31
32	MS 02328-0400	0.187	0.087	4	0.025	0.070	6	0.218	0.064	4	96/12/21	98/01/16
34	Q 0235+0121	-0.002	0.066	5	0.108	0.075	5	-0.032	0.070	3	96/12/02	98/01/04
35	Q 0238-0142	0.246	0.074	5	0.103	0.064	5	0.109	0.045	5	96/12/08	98/02/17
37	US 3150	-0.259	0.073	5	–	–	–	–	–	–	96/11/25	98/01/06
38	MS 02448+1928	-0.101	0.025	8	-0.056	0.035	6	0.071	0.029	7	96/12/01	97/12/27
42	US 3376	-0.114	0.129	1	–	–	–	–	–	–	96/12/22	97/02/22
44	US 3472	-0.096	0.075	5	-0.090	0.053	4	-0.280	0.059	6	96/12/22	97/12/31
45	S 0257-0027	0.070	0.142	7	-0.336	0.192	7	0.000	0.060	6	97/02/09	98/01/21
50	Q 0305+0222	-0.044	0.062	6	0.156	0.076	6	-0.108	0.074	5	96/12/02	98/02/09
51	PKS 0306+102	–	–	–	–	–	–	0.859	0.083	5	96/12/23	98/01/26
54	MS 03120+1405	-0.030	0.044	8	-0.007	0.085	7	0.127	0.075	7	96/12/09	98/01/29
56	B2 0321+33	0.159	0.015	24	0.197	0.019	19	0.158	0.018	12	96/02/05	98/01/05
59	3C 93.0	-0.126	0.052	9	-0.045	0.058	10	-0.025	0.047	10	97/02/04	98/01/05
61	PKS 0353+027	0.000	0.057	11	0.013	0.059	16	0.060	0.062	13	97/01/22	98/01/16
62	MS 03574+1046	-0.137	0.034	4	-0.361	0.035	7	-0.276	0.032	6	96/12/01	97/12/24
64	MS 04124-0802	-0.123	0.015	6	-0.162	0.030	7	-0.107	0.024	5	96/02/06	97/12/27
65	3C 110	-0.048	0.035	8	-0.063	0.064	5	-0.014	0.061	7	96/02/02	97/12/31

Table 1-Continued.

Number	Name	ΔJ	$\sigma_{\Delta J}$	n_J	ΔH	$\sigma_{\Delta H}$	n_H	$\Delta K'$	$\sigma_{\Delta K'}$	$n_{K'}$	date1	date2
66	PKS 0420-01	0.736	0.079	7	0.677	0.070	6	0.690	0.051	4	96/12/08	97/12/24
67	3C 120	0.044	0.014	14	-0.079	0.018	11	-0.165	0.034	6	96/02/05	97/12/27
68	IRAS 04448-0513	0.053	0.014	9	0.060	0.021	8	0.150	0.043	6	96/02/05	97/12/27
69	Q 0446+0130	–	–	–	–	–	–	0.123	0.085	8	97/01/20	98/01/31
71	UGC 3223	-0.305	0.110	3	-0.058	0.016	9	–	–	–	96/02/06	97/12/27
72	2E 0507+1626	0.007	0.083	1	–	–	–	0.468	0.152	1	96/02/06	97/12/27
73	3C 135.0	-0.035	0.030	18	0.053	0.037	17	0.070	0.042	16	96/12/07	97/12/31
74	AKN 120	-0.177	0.072	22	-0.145	0.011	16	-0.124	0.014	11	96/02/05	98/01/06
75	1E 0514-0030	0.080	0.044	19	0.163	0.048	14	0.011	0.031	18	96/02/11	97/12/24
76	3C 138.0	-0.070	0.067	48	–	–	–	–	–	–	97/01/06	98/01/24
77	3C 147.0	-0.237	0.029	24	-0.168	0.036	25	-0.171	0.039	18	96/12/21	98/01/05
78	4C 16.14	-0.491	0.198	70	–	–	–	–	–	–	96/12/07	98/02/08
79	MCG 08.11.11	-0.483	0.012	59	-0.668	0.011	24	-0.628	0.055	16	96/02/03	98/01/06
81	3C 154.0	0.126	0.032	62	0.212	0.035	61	-0.022	0.030	50	96/12/09	97/12/31
82	MC 0657+176	0.022	0.075	57	–	–	–	0.081	0.097	40	97/01/06	98/02/06
83	3C 175.0	0.094	0.029	3	0.205	0.052	12	0.465	0.065	10	96/11/29	98/01/04
84	B2 0709+37	0.315	0.067	17	-0.284	0.040	16	-0.377	0.046	20	96/02/02	98/01/05
85	MARK 376	0.112	0.011	33	0.140	0.012	25	0.383	0.069	15	96/02/03	98/01/05
88	PKS 0736+01	0.100	0.035	20	0.098	0.040	20	-2.699	0.111	1	96/01/31	97/12/18
89	OI 363	-0.210	0.045	19	-0.150	0.076	18	–	–	–	96/01/31	98/01/06
91	B2 0742+31	-0.225	0.099	18	-0.200	0.102	18	-0.441	0.043	13	96/01/24	97/12/24
93	GC 0742+33	0.070	0.074	19	-0.150	0.073	19	–	–	–	96/12/21	98/01/21
95	RXS J07498+3454	-0.016	0.060	9	0.090	0.069	5	0.149	0.055	6	96/12/03	98/01/05
96	PKS 0748+126	0.461	0.069	13	0.641	0.063	13	0.521	0.050	16	97/01/26	98/01/16
98	B2 0752+25A	-0.055	0.051	6	0.003	0.090	3	-0.182	0.124	2	96/01/31	97/12/31
99	B3 0754+394	0.173	0.146	17	0.126	0.107	5	0.058	0.011	11	96/01/24	98/01/05
101	UGC 4155	-0.086	0.059	14	-0.068	0.013	12	-0.030	0.014	6	96/02/06	97/12/24
102	MARK 1210	-0.150	0.015	25	0.063	0.014	17	-0.030	0.026	15	96/02/05	98/01/05
103	MS 08019+2129	-0.030	0.022	12	-0.032	0.030	6	0.000	0.027	6	96/01/24	97/12/18
104	3C 192.0	-0.144	0.138	3	-0.118	0.139	2	0.020	0.087	1	96/12/03	97/12/18
105	MS 08080+4840	-0.166	0.048	16	-0.147	0.087	14	0.052	0.083	16	96/12/31	98/02/10
109	RX J08166+2941	0.291	0.097	15	–	–	–	0.604	0.107	15	96/12/07	98/01/19
110	3C 197	0.094	0.036	20	0.072	0.105	17	0.044	0.063	16	97/01/26	98/01/26

Table 1-Continued.

Number	Name	ΔJ	$\sigma_{\Delta J}$	n_J	ΔH	$\sigma_{\Delta H}$	n_H	$\Delta K'$	$\sigma_{\Delta K'}$	$n_{K'}$	date1	date2
111	RXS J08223+3305	-0.005	0.038	4	0.061	0.070	4	-0.008	0.042	6	97/02/20	98/01/16
112	KUV 08217+4235	–	–	–	–	–	–	-0.037	0.127	2	96/11/29	97/12/31
113	4C 44.17	0.161	0.049	12	0.347	0.094	14	0.377	0.428	12	97/01/27	98/02/09
115	B2 0827+24	-0.712	0.046	14	-0.302	0.111	13	-0.394	0.049	14	96/12/07	98/01/16
116	PG 0832+251	-0.148	0.032	9	-0.155	0.051	8	-0.075	0.019	9	96/01/24	97/12/24
118	US 1329	-0.541	0.030	10	-0.489	0.044	6	-0.463	0.073	7	96/02/02	97/12/25
119	MARK 1218	-0.094	0.028	2	-0.456	0.128	3	-0.179	0.139	3	96/02/05	97/12/24
122	KUV 08377+4136	-0.516	0.079	10	0.573	0.148	9	–	–	–	96/12/22	98/02/08
123	PG 0844+349	-0.067	0.018	9	-0.023	0.030	6	-0.115	0.059	3	96/02/02	97/12/24
124	55W 179	–	–	–	–	–	–	-0.196	0.179	2	97/02/12	98/03/18
125	CSO 2	-0.034	0.032	6	0.128	0.052	9	0.008	0.044	8	96/12/07	98/01/06
127	LB 8741	0.188	0.057	15	–	–	–	0.188	0.084	8	96/12/07	98/01/24
129	US 1786	–	–	–	0.118	0.111	1	0.127	0.061	8	96/12/22	98/01/21
131	MS 08498+2820	0.001	0.056	7	-0.100	0.064	11	-0.068	0.294	4	97/02/19	98/01/30
132	MS 08502+2825	0.036	0.090	12	0.026	0.094	12	0.089	0.084	10	96/12/02	98/01/29
133	US 1867	-0.258	0.045	7	-0.262	0.059	8	-0.141	0.048	4	96/02/07	97/12/25
135	NGC 2683 U1	0.343	0.303	3	-0.149	0.139	4	0.162	0.085	4	96/12/08	98/01/19
136	LB 8948	-0.023	0.051	7	0.057	0.047	8	0.035	0.023	6	96/12/07	97/12/24
137	LB 8960	0.058	0.054	7	–	–	–	0.294	0.109	7	96/12/07	98/01/30
138	US 2068	-0.149	0.039	4	–	–	–	0.006	0.127	4	96/11/29	98/01/21
139	KUV 09012+4019	-0.005	0.159	5	–	–	–	0.115	0.041	7	97/02/22	98/04/03
140	US 44	-0.045	0.025	9	-0.050	0.027	8	-0.094	0.031	5	97/02/11	97/12/27
141	1E 0906+4254	-0.010	0.049	11	-0.267	0.070	12	0.058	0.081	7	96/12/30	98/03/02
142	4C 05.38	-0.009	0.046	7	-0.133	0.140	6	-0.062	0.042	4	96/12/02	98/01/02
143	MARK 704	0.036	0.025	3	0.048	0.021	3	0.111	0.036	4	96/02/03	97/12/24
144	RXS J09189+3016	-0.185	0.132	10	-0.173	0.075	9	-0.228	0.078	9	97/02/20	98/01/26
146	E 0917+341	-0.053	0.078	2	-0.032	0.073	2	-0.169	0.121	2	97/02/23	98/03/02
148	PG 0923+201	-0.186	0.021	6	-0.257	0.030	4	-0.201	0.088	3	96/02/01	97/12/25
149	MARK 705	0.093	0.019	8	0.503	0.038	13	0.221	0.017	10	96/02/06	97/12/24
150	B2 0923+39	0.020	0.065	3	-0.293	0.106	1	–	–	–	96/12/21	98/03/15
152	MS 09309+2128	–	–	–	-0.721	0.120	1	-0.473	0.160	1	96/11/30	97/12/27
153	US 737	-0.016	0.034	13	0.167	0.046	13	-0.152	0.031	12	96/02/02	97/12/27
154	MARK 707	–	–	–	0.199	0.047	2	0.120	0.048	3	96/02/03	97/12/24

Table 1-Continued.

Number	Name	ΔJ	$\sigma_{\Delta J}$	n_J	ΔH	$\sigma_{\Delta H}$	n_H	$\Delta K'$	$\sigma_{\Delta K'}$	$n_{K'}$	date1	date2
155	TON 1078	0.033	0.041	5	0.025	0.057	4	0.051	0.087	1	96/02/02	98/01/05
156	PG 0936+396	-0.122	0.064	7	-0.657	0.205	4	-0.398	0.239	3	96/02/02	98/02/12
157	US 822	0.016	0.037	4	0.069	0.056	4	0.016	0.049	5	96/12/09	98/01/26
159	HS 0940+4820	–	–	–	0.117	0.212	4	0.108	0.051	6	96/12/29	98/01/29
160	2E 0944+4629	0.100	0.057	9	-0.043	0.084	8	0.072	0.077	11	97/01/02	98/02/10
161	US 995	0.023	0.038	7	0.077	0.047	4	0.081	0.162	3	96/02/10	97/12/27
162	HS 0946+4845	-0.322	0.049	3	-0.328	0.093	3	0.041	0.086	3	96/11/29	98/02/10
164	US 1107	-0.470	0.044	2	-0.517	0.054	3	-0.673	0.123	2	96/11/29	98/01/16
165	PG 0953+415	-0.128	0.024	7	-0.181	0.032	6	-0.226	0.030	4	96/02/02	97/12/18
166	3C 232	-0.073	0.030	7	-0.054	0.049	4	-0.207	0.045	7	96/02/02	98/01/05
167	NGC 3080	0.122	0.015	14	0.207	0.079	10	0.188	0.061	7	96/02/03	97/12/24
168	IRAS 09595-0755	-0.555	0.018	8	–	–	–	-0.730	0.075	1	96/02/11	97/12/25
170	KUV 10000+3255	0.248	0.272	4	–	–	–	-0.362	0.224	5	96/11/30	98/02/06
172	PG 1001+05	0.015	0.074	8	0.288	0.066	5	0.188	0.029	5	96/02/10	97/12/24
173	PKS 1004+13	0.393	0.153	5	0.026	0.052	4	-0.058	0.035	3	96/02/01	97/12/18
174	RXS J10079+4918	0.205	0.051	3	0.147	0.161	3	0.277	0.130	3	97/02/20	98/01/19
175	TON 488	0.733	0.072	3	–	–	–	–	–	–	96/01/30	96/04/05
177	Q 1008+0058	-0.186	0.244	2	0.026	0.097	1	-0.112	0.137	2	96/02/10	96/11/30
179	TON 1187	-0.050	0.030	8	-0.057	0.038	7	0.037	0.020	9	96/01/30	97/12/24
180	PG 1011-040	0.053	0.021	12	0.139	0.025	11	0.235	0.029	6	96/02/11	97/12/25
181	PKS 1011+23	-0.315	0.043	5	-0.283	0.052	6	-0.298	0.048	6	96/12/08	98/01/21
182	PG 1012+008	-0.014	0.376	8	-0.114	0.038	5	-0.070	0.024	7	96/02/01	97/12/18
190	Q 1047+067	–	–	–	-0.029	0.059	4	0.022	0.039	3	96/11/30	97/12/25
191	MS 10470+3537	0.298	0.082	5	-0.222	0.090	4	-0.081	0.052	4	96/12/29	98/01/16
193	PG 1049-005	0.045	0.043	8	0.002	0.050	9	-0.047	0.034	4	96/02/12	97/12/18
194	MARK 634	0.074	0.073	1	–	–	–	–	–	–	96/02/03	97/12/25
196	RXS J11008+2839	0.095	0.308	3	0.000	0.222	2	0.083	0.078	2	97/02/22	98/01/19
197	MARK 728	0.174	0.039	9	0.062	0.053	4	0.270	0.039	5	96/02/03	97/12/25
198	TOL 1059+105	-0.292	0.037	5	-0.319	0.262	5	-0.329	0.042	7	96/02/05	97/12/27
199	1059.6+0157	–	–	–	–	–	–	-0.043	0.081	5	97/01/03	98/02/06
200	PKS 1103-006	0.032	0.048	7	0.110	0.068	6	-0.074	0.066	5	96/02/12	98/01/05
201	MC 1104+167	-0.815	0.036	8	-0.821	0.057	8	-0.666	0.045	12	96/02/02	98/01/19
204	PG 1115+407	-0.154	0.021	7	-0.015	0.182	8	-0.130	0.074	8	96/02/12	98/04/03

Table 1-Continued.

Number	Name	ΔJ	$\sigma_{\Delta J}$	n_J	ΔH	$\sigma_{\Delta H}$	n_H	$\Delta K'$	$\sigma_{\Delta K'}$	$n_{K'}$	date1	date2
205	PG 1116+215	-0.053	0.026	4	0.041	0.027	4	–	–	–	96/02/02	98/01/06
206	MARK 734	-0.041	0.016	5	-0.013	0.027	6	0.038	0.084	3	96/02/05	97/12/24
210	MARK 423	0.134	0.133	1	–	–	–	–	–	–	96/02/06	98/01/02
211	US 2450	-0.007	0.036	8	-0.094	0.053	7	0.036	0.039	9	97/02/22	98/01/24
212	MARK 1298	-0.174	0.211	5	–	–	–	0.213	0.203	3	96/02/06	98/01/24
213	MARK 1447	0.114	0.038	6	-0.060	0.027	6	-0.083	0.028	6	96/02/05	97/12/24
217	MCG 06.26.012	0.090	0.023	2	–	–	–	0.139	0.107	2	96/02/05	97/12/24
218	MARK 744	-0.142	0.155	2	–	–	–	-0.091	0.186	1	96/02/06	98/01/24
219	WAS 26	-0.086	0.030	9	0.552	0.076	7	-0.050	0.044	5	96/02/02	97/12/18
220	CG 855	-0.234	0.039	3	-0.145	0.105	1	-0.170	0.133	1	96/02/05	98/01/02
222	MC 1146+111	0.090	0.047	7	–	–	–	-0.209	0.139	5	96/12/08	98/03/07
227	GQ COM	-0.244	0.048	7	0.103	0.043	8	0.083	0.027	6	96/01/31	97/12/18
228	UGC 7064	-0.393	0.038	8	-0.065	0.022	3	-0.138	0.014	5	96/02/12	98/01/02
230	PG 1211+143	0.158	0.043	4	0.153	0.029	3	0.052	0.012	3	96/01/31	98/01/24
232	PKS 1216-010	-0.335	0.075	8	-0.401	0.104	4	–	–	–	96/02/02	98/01/21
233	MARK 1320	-0.701	0.031	5	-0.551	0.036	5	-0.388	0.066	3	96/02/11	97/12/27
235	Q 1220+0939	0.138	0.070	4	-0.183	0.143	4	–	–	–	96/12/21	98/01/30
236	MS 12209+1601	-0.319	0.029	6	-0.386	0.044	8	-0.201	0.045	6	96/02/06	98/01/21
238	2E 1224+0930	-0.129	0.052	2	-0.021	0.105	1	-0.114	0.226	2	97/01/20	98/01/31
239	3C 273.0	0.320	0.024	5	0.378	0.013	4	0.251	0.256	7	96/01/30	98/01/24
241	TON 1542	-0.031	0.071	5	-0.061	0.067	4	0.028	0.030	4	96/02/06	98/01/02
242	CSO 150	-0.135	0.059	9	–	–	–	-0.009	0.082	4	96/01/30	96/02/21
243	IC 3528	0.126	0.067	5	–	–	–	-1.787	0.222	1	96/02/06	97/12/25
247	WAS 61	-0.598	0.018	5	-0.580	0.071	6	-0.490	0.020	8	96/02/11	98/01/02
248	Q 1240+1546	0.077	0.113	3	0.180	0.102	1	-0.151	0.199	1	96/02/06	98/01/02
249	CBS 63	–	–	–	–	–	–	0.021	0.137	2	97/02/23	98/02/12
250	Q 1240+1746	-0.082	0.076	6	-0.163	0.106	7	-0.319	0.092	6	96/12/31	98/03/18
251	4C 45.26	0.276	0.090	5	–	–	–	0.245	0.133	4	96/12/21	98/02/02
257	3C 281	0.153	0.063	3	-0.033	0.085	3	-0.154	0.109	3	97/02/23	98/01/30
260	CSO 835	-0.172	0.092	2	0.116	0.144	1	–	–	–	97/02/01	97/02/06
262	PG 1309+355	0.020	0.128	4	1.578	0.488	4	0.124	0.114	2	96/02/02	98/03/01
263	RXS J13129+2628	0.090	0.017	9	0.096	0.034	6	0.043	0.030	6	96/12/29	98/01/29
264	Q 1316+0103	-0.131	0.082	7	-0.029	0.088	9	0.028	0.181	9	97/01/30	98/02/10

Table 1-Continued.

Number	Name	ΔJ	$\sigma_{\Delta J}$	n_J	ΔH	$\sigma_{\Delta H}$	n_H	$\Delta K'$	$\sigma_{\Delta K'}$	$n_{K'}$	date1	date2
265	MARK 1347	-0.010	0.013	10	-0.059	0.014	9	-0.048	0.015	7	96/02/06	98/01/26
266	Q 1326-0516	-0.070	0.026	5	-0.005	0.049	5	0.030	0.037	5	96/01/30	98/01/31
267	MS 13285+3135	0.367	0.111	5	0.320	0.169	2	0.363	0.162	2	97/02/20	98/01/24
271	IRAS 13349+2438	-0.079	0.013	7	0.035	0.057	3	0.106	0.079	2	96/02/10	98/01/24
272	Q 1338-0030	–	–	–	0.144	0.101	1	-0.063	0.103	1	97/02/23	98/01/30
273	TON 730	0.097	0.042	6	0.121	0.044	6	0.388	0.029	6	96/02/06	97/12/18
274	MARK 69	0.023	0.027	5	0.063	0.266	4	–	–	–	96/02/05	98/03/02
276	MARK 662	-0.084	0.099	2	-0.077	0.131	2	–	–	–	96/02/06	98/01/31
278	MARK 463E	0.016	0.015	7	0.066	0.039	5	-0.056	0.129	7	96/02/06	98/01/31
279	PG 1402+261	0.265	0.019	6	0.363	0.048	3	0.285	0.080	2	96/02/10	98/01/26
280	PG 1404+226	-0.097	0.023	6	-0.147	0.034	5	-0.093	0.031	4	96/02/10	98/03/02
281	OQ 208	0.126	0.016	8	0.302	0.058	6	0.128	0.156	1	96/02/06	98/01/26
283	PG 1407+265	-0.055	0.038	5	-0.090	0.038	5	0.123	0.054	5	96/01/31	98/02/12
284	PG 1411+442	-0.108	0.013	5	-0.071	0.014	6	-0.061	0.014	4	96/02/10	98/03/02
285	PG 1415+451	-0.047	0.016	10	-0.059	0.022	10	-0.025	0.031	5	96/02/10	98/03/02
286	NGC 5548	–	–	–	0.100	0.133	1	0.189	0.376	4	96/02/12	98/01/31
287	H 1419+480	-0.175	0.015	11	-0.241	0.019	10	-0.297	0.014	9	96/02/12	98/03/02
290	MARK 471	0.038	0.013	6	0.029	0.055	5	0.021	0.026	4	96/02/12	98/03/02
291	B 1422+231	0.077	0.019	8	0.108	0.033	7	0.072	0.027	5	97/02/19	98/03/01
292	2E 1423+2008	–	–	–	–	–	–	0.003	0.100	1	96/02/10	98/01/02
293	MARK 813	-0.187	0.017	6	-0.216	0.026	6	-0.208	0.104	2	96/01/30	98/02/08
294	B2 1425+26	0.021	0.060	6	0.203	0.338	3	–	–	–	96/01/30	98/02/12
295	MARK 1383	-0.266	0.054	2	-0.081	0.013	3	-0.089	0.038	2	96/02/22	98/02/02
296	MARK 684	-0.426	0.096	14	-0.010	0.016	9	0.028	0.024	5	96/02/06	98/01/26
298	MARK 474	0.059	0.027	12	0.010	0.029	8	0.110	0.028	7	96/02/12	98/03/01
300	MARK 478	-0.090	0.135	14	-0.126	0.013	10	-0.138	0.016	12	96/02/10	98/03/02
301	PG 1444+407	-0.169	0.030	7	-0.026	0.027	8	-0.005	0.024	8	96/02/10	96/04/05
302	Q 1446-0035	0.124	0.073	5	0.234	0.069	5	0.050	0.112	3	97/02/06	98/03/15
303	PG 1448+273	-0.074	0.014	13	-0.061	0.017	8	-0.001	0.021	8	96/02/10	98/03/02
304	MS 14564+2147	-0.407	0.025	9	-0.597	0.078	11	-0.657	0.041	6	96/02/12	98/03/02
306	MARK 841	0.363	0.037	6	0.391	0.330	2	–	–	–	96/02/12	98/02/02
308	PKS 1509+022	0.054	0.034	10	0.138	0.052	13	0.063	0.044	9	97/02/24	98/03/15
309	MS 15198-0633	-0.265	0.020	14	-0.194	0.022	11	-0.270	0.018	9	96/02/22	98/03/07

Table 1-Continued.

Number	Name	ΔJ	$\sigma_{\Delta J}$	n_J	ΔH	$\sigma_{\Delta H}$	n_H	$\Delta K'$	$\sigma_{\Delta K'}$	$n_{K'}$	date1	date2
310	LB 9695	-0.284	0.085	11	–	–	–	–	–	–	97/01/30	98/03/17
311	OR 139	-0.086	0.061	7	0.039	0.063	7	0.100	0.091	8	97/01/28	98/02/06
312	QNZ5:02	0.003	0.054	9	0.023	0.070	8	-0.037	0.046	6	97/02/23	98/02/12
313	MARK 1098	-0.100	0.012	13	-0.136	0.015	12	-0.135	0.018	5	96/02/10	98/02/02
314	NGC 5940	-0.153	0.014	14	-0.237	0.139	9	-0.123	0.019	4	96/02/22	98/01/31
315	KUV 15524+2153	-0.082	0.038	11	-0.014	0.038	13	-0.081	0.043	10	97/02/22	98/03/16
318	PG 1634+706	0.074	0.011	9	0.055	0.017	9	–	–	–	97/02/22	98/03/07
319	RXS J16446+2619	-0.042	0.080	8	-0.117	0.055	9	0.127	0.308	8	97/02/11	98/03/16
320	TEX 1652+151	-0.130	0.047	15	0.100	0.093	14	0.041	0.042	13	97/02/20	98/03/16
321	2E 1654+3514	–	–	–	0.215	0.133	8	-0.067	0.108	8	97/02/20	98/03/18
323	PKS 1739+18C	-0.141	0.029	24	0.167	0.031	22	0.095	0.024	13	97/02/24	98/03/07
328	3C 459.0	-0.085	0.063	4	0.248	0.102	5	-0.014	0.062	3	96/11/25	97/12/31
330	PB 5577	-0.192	0.098	5	0.047	0.116	3	-0.079	0.113	3	96/12/02	97/12/27
331	Q 2352+0025	0.052	0.048	8	0.033	0.053	7	0.022	0.035	6	96/12/23	97/12/31

Note. — The sequential number in the first column is the same as in the object list in Paper I. The numbers n_J , n_H , and $n_{K'}$ represent those of reference objects used in the differential photometry in the J , H , and K' bands, respectively.

Table 1. Ratio of varied AGNs with 2σ and 3σ confidence.

Sample	J			H			K'		
	$> 2\sigma$	$> 3\sigma$	n	$> 2\sigma$	$> 3\sigma$	n	$> 2\sigma$	$> 3\sigma$	n
all AGNs	61%	47%	165	58%	42%	134	56%	42%	135
$\sigma_{\Delta m_{AGN}} < 0.03$	85%	73%	52	82%	67%	33	73%	65%	37
$0.03 < \sigma_{\Delta m_{AGN}} < 0.05$	59%	44%	54	68%	50%	34	60%	43%	47
$0.05 < \sigma_{\Delta m_{AGN}} < 0.10$	41%	27%	59	40%	27%	67	41%	26%	51
radio quiet AGNs	59%	47%	116	60%	42%	97	59%	41%	100
$\Delta t_{rest} = 100 - 400days$	38%	27%	49	32%	11%	38	41%	14%	42
$\Delta t_{rest} = 400 - 800days$	75%	61%	67	78%	63%	59	72%	60%	58
radio loud AGNs	67%	48%	42	50%	41%	32	44%	41%	32
$\Delta t_{rest} = 100 - 400days$	60%	43%	30	48%	38%	21	36%	32%	25
$\Delta t_{rest} = 400 - 800days$	83%	58%	12	55%	46%	11	71%	71%	7

Note. — The number n represents that of AGNs in each sample.